Math. Model. Nat. Phenom.
Vol. 7, No. 1, 2012, pp. 78-104
DOI: 10.1051/mmnp/20127105

A Hybrid Model Describing Different Morphologies of Tumor Invasion Fronts

M. Scianna[1,2] **and L. Preziosi**[1*]

[1] Department of Mathematics, Politecnico di Torino
Corso Duca degli Abruzzi 24, 10129 Torino, Italy
[2] Institute for Cancer Research and Treatment
Strada Provinciale 142, 10060 Candiolo, Italy

Abstract. The invasive capability is fundamental in determining the malignancy of a solid tumor. Revealing biomedical strategies that are able to partially decrease cancer invasiveness is therefore an important approach in the treatment of the disease and has given rise to multiple *in vitro* and *in silico* models. We here develop a hybrid computational framework, whose aim is to characterize the effects of the different cellular and subcellular mechanisms involved in the invasion of a malignant mass. In particular, a discrete Cellular Potts Model is used to represent the population of cancer cells at the mesoscopic scale, while a continuous approach of reaction-diffusion equations is employed to describe the evolution of microscopic variables, as the nutrients and the proteins present in the microenvironment and the matrix degrading enzymes secreted by the tumor. The behavior of each cell is then determined by a balance of forces, such as homotypic (cell-cell) and heterotypic (cell-matrix) adhesions and haptotaxis, and is mediated by the internal state of the individual, i.e. its motility. The resulting composite model quantifies the influence of changes in the mechanisms involved in tumor invasion and, more interestingly, puts in evidence possible therapeutic approaches, that are potentially effective in decreasing the malignancy of the disease, such as the alteration in the adhesive properties of the cells, the inhibition in their ability to remodel and the disruption of the haptotactic movement. We also extend the simulation framework by including cell proliferation which, following experimental evidence, is regulated by the intracellular level of growth factors. Interestingly, in spite of the increment in cellular density, the depth of invasion is not significantly increased, as one could have expected.

Key words: cellular potts model · tumor invasion · matrix metalloproteinases

*Corresponding author. E-mail: luigi.preziosi@polito.it

AMS subject classification: 97M60

1. Introduction

Solid tumors are thought to arise from small nodes of cells that have undergone genetic mutations and/or epigenetic alterations, able to escape from DNA repair mechanisms and to cause abnormal growth regulatory mechanisms [3, 49]. Such primary malignant colonies undergo through a relatively simple, avascular stage of growth, with nutrient and growth factor supply by diffusion from the local microenvironment [3, 47, 72]. However, a further search of available quantities of critical substrates results in a subsequent aggressive phase, with the invasion of the surrounding tissue [3, 10]. In particular, as reproduced in Fig. 1, a part of the malignant mass remains densely packed, while a number of isolated cells detach and begin to invade the neighboring spaces. These individuals are less adhesive, highly mobile and metabolically active, due to the fact that they experience a high level of chemical factors, and are able to secrete an enhanced quantity of matrix degrading enzymes (MDEs) [32, 68]. In particular, the production of proteolytic enzymes, such as matrix metalloproteinases (MMPs), is essential during the invasive phase: the dissolution of the ECM provides in fact both a space into which aggressive cells can move and a gradient which can be used by the cells themselves to direct their movement (i.e., haptotaxis), see [14, 48, 68]. The scattered individuals, evading destruction by the immune system, may subsequently enter the host bloodstream or lymphatics, extravasate at a distant site, and establish secondary colonies with devastating consequences for the wellbeing of the patient, as the likelihood of success of therapeutic interventions strongly decreases, as modeled in [25, 55].

A deep understanding of the regulatory dynamics of the invasive phase of tumor development, in particular of the morphological instability resulting in the shed of single cells, represents therefore a fundamental issue in cancer research, as also commented in [15]. However, the relative importance of the cellular and molecular processes involved has not been completely revealed yet. In particular, an accurate and quantitative relation of their effects on the overall malignancy of the disease has been demonstrated to be unfeasible using only laboratory-based methods. In last decades a fundamental help has been provided by computational approaches, able to realistically reproduce selected features of the biological system and to test potential anti-tumoral strategies, as pointed out by the books [12, 39] and by the excellent reviews [6, 8, 13, 29, 38, 40, 54, 53, 70]. The variety of numerical methods now available for performing simulations of nonlinear solid tumor growth and invasion has been typically based on either continuous or discrete approaches. Among continuous techniques, single-phase models deal with tumor front invasion and surface growth, as reviewed in [11, 14, 38, 70], while multi-phase mixture present tumor interface instabilities, see [6, 42, 52]. However, all these approaches overlook the behavior and the mutual interactions of single cells, which, as seen, are fundamental in determining the invasiveness of cancers and the subsequent metastatization. Discrete techniques, which include cellular automata and agent-based models [2, 4, 34, 37, 44, 56, 71], are instead able to preserve the identity of each simulated indi-

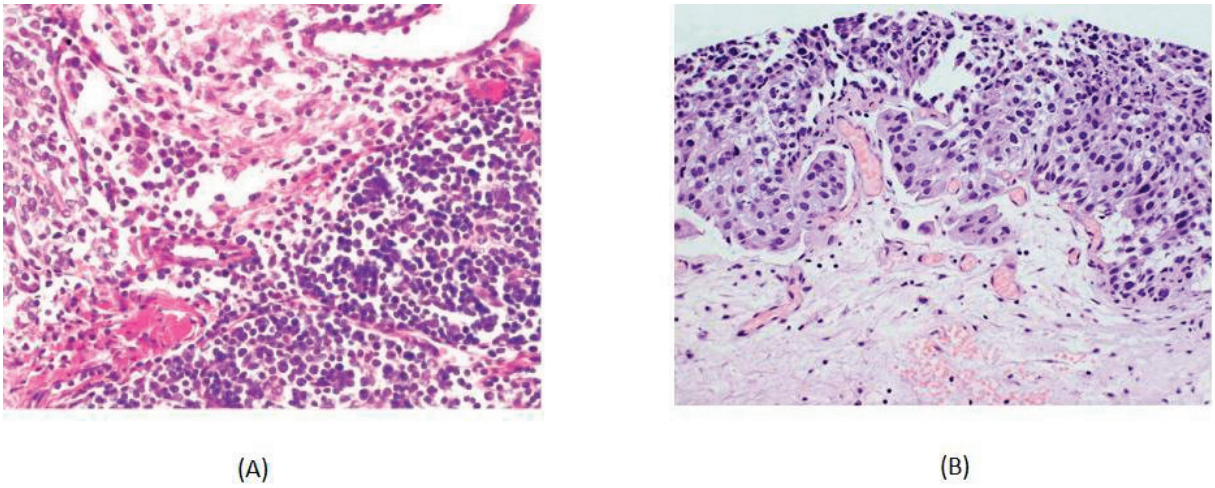

Figure 1: A high-power photomicrographs showing microinvasive solid tumors. (A) Single aggressive malignant cells of a type B2 thymoma detaching from the main malignant mass, located in the anterior mediastinum and myasthenia gravis. (B) pT1 urothelial carcinoma invading into the lamina propria. In both cases, it is possible to notice single isolated cells or irregular small clusters of cells invading the surrounding tissue. Image (A) courtesy of the Institute for Cancer Research and Treatment of Candiolo (I.R.C.C.), image (B) taken from `www.visualhistology.com`.

vidual, to more naturally capture their biophysical properties, such as shape change, adhesion and intrinsic motility, and to handle local dynamics. On the contrary, purely discrete models translate complex microscopic processes into simple phenomenological rules, are difficult to study analytically and the associated computational cost rapidly increases with the number of cells modeled, which makes it difficult to simulate lesions longer than one millimeter.

In recent years, hybrid continuum-discrete approaches have been developed and have shown the potential to combine the best features of both types of techniques and the capability to realistically deals with the multiple scales involved in tumor invasion [5, 23, 24]. We here follow this way and present a composite multi-level modeling framework to reproduce and quantitatively analyze the first phase of tumor invasion. In particular, we aim to focus on the emergence of different morphologies at the front of tumor invasion, which result both from cell-based processes (such as cell elasticity, adhesive properties and motility) and from subcellular molecular dynamics (such as growth factor internalization, ECM protein digestion and MMP secretion). Indeed, the malignant cell mass is represented at the mesoscopic level with an extended Cellular Potts Model (CPM), see for instance [7, 26, 27, 28, 43, 62], a lattice-based Monte Carlo technique employing a stochastic energy minimization to display the evolution of the cell culture over time, while the evolution of the microenvironmental components (such as the transport of growth factors and the mutual dynamics of tumor-secreted MMPs and ECM proteins) is modeled by continuous reaction-diffusion equations. The resulting model is able to characterize the morphology of the invasive tumor and to quantify its malignancy in term of invasive depth in several different conditions. Furthermore, the proposed approach has the potential to make clear the relevance of the various mechanisms

involved and to suggest possible intervention strategies able to reduce the aggressiveness of the lesion by controlling its morphological stability.

The rest of this paper is organized as follows. In Section 2, we clarify the assumptions on which our approach is based. The computational findings are then shown in Section 3, and discussed in Section 4.

2. Mathematical Model

We elaborate a hybrid, multilevel modeling framework for tumor invasion, which is based on the extensions of the Cellular Potts Model reviewed in [62]. The aim is a simulation environment in which the cellular and multicellular behavior autonomously emerges, rather than being imposed a priori by a set of phenomenological rules. In particular, the malignant cells are represented by physical discrete objects, that locally interact with each other and with the microenvironment through their membranes. The molecular biology is instead incorporated with a macroscopic description of the evolution of nutrients, ECM proteins and tumor matrix metalloproteinasis, see Fig. 2 for a schematic representation. As a key feature of our discrete-continuum composite approach, the different scales affects each other, as the distribution of nutrients and ECM proteins in the extracellular environment influence cells' properties and phenomenology (with carefully-calibrated constitutive relations).

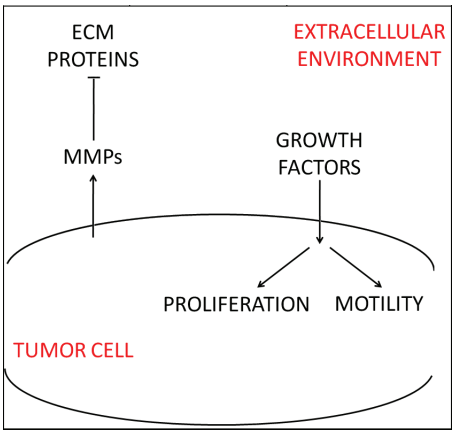

Figure 2: Schematic diagram of the key processes included in the mathematical model. The extracellular environment provides to tumor cells soluble growth factors, whose uptake enhances cell intrinsic motility and proliferation. Tumor cells, in turn, secrete matrix metalloproteinases (MMPs), which degrade ECM proteins.

2.1. Extended Cellular Potts Model

The invasion of the tumor mass is modeled at the mesoscopic level using an extended Cellular Potts Model, a grid-based stochastic approach, which realistically preserves the identity of single individuals and describes their behavior and mutual interactions in energetic terms and constraints. The simulation domain is a lattice (i.e., a regular numerical repeated graphs) Ω, where each site $\mathbf{x} \in \Omega$ is labeled by an integer number, $j(\mathbf{x})$, that can be interpreted as a degenerate *spin* originally coming from statistical physics [33, 51]. As classically adopted in CPM models, a neighboring site of $\mathbf{x}$ is denoted by $\mathbf{x}'$ and its overall neighborhood by $\Omega'_{\mathbf{x}}$, i.e. $\Omega'_{\mathbf{x}} = \{\mathbf{x}' \in \Omega : \mathbf{x}' \text{ is a neighbor of } \mathbf{x}\}$. Subdomains of contiguous sites with identical spin form single discrete objects, which are characterized by an object type, $\tau(j)$. The cancer cells, i, are here defined as compartmentalized units, composed of two subregions: the cell nucleus, a central more or less round cluster of type $\tau = N$, whose location and geometry is estimated with experimental images, and the surrounding cytosol, $\tau = C$, see Fig. 3. Each cell compartment is obviously characterized, as an additional attribute, by the cluster id i to identify the individual it belongs to. The tumor mass resides in an extracellular matrix, $\tau = M$, which is assumed to be isotropically distributed throughout the simulation domain, forming no large-scale structures. It reproduces in fact the mixture of soluble components (among others, long carbohydrate polymers, and non-proteoglycan polysaccharides), which, together with the water solvent, compose the so-called interstitial medium.

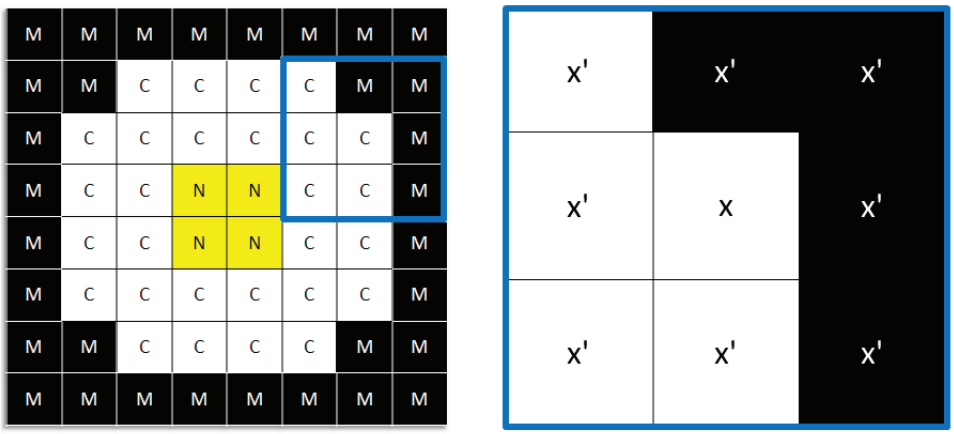

Figure 3: Representation of a compartmentalized cell i. Lattice sites of the nuclear region $\tau(j(\mathbf{x}) = N)$ are in yellow, lattice sites of the cytosol in white $\tau(j(\mathbf{x}) = C)$. The extracellular matrix is labeled with $\tau = M$, and is colored in black. In the zoom view it is possible to see a sub-plasmamembrane lattice site, $\mathbf{x}$, and its first-nearest neighbors, $\mathbf{x}' \in \Omega'_{\mathbf{x}}$.

The malignant cells move and behave to iteratively and stochastically reduce the free energy of the overall system, given by the *hamiltonian* H, whose expression will be clarified below. The core algorithm is a modified Metropolis method for Monte Carlo dynamics [28, 45], which is able to implement the natural exploratory behavior of cells, reproducing their cytoskeletally-driven membrane fluctuations and extensions of pseudopods. Procedurally, at each time step t, called Monte Carlo Step (MCS, the basic unit of time of the discrete model), a lattice site, $\mathbf{x}_{source}$, is selected

at random and assigns its spin, $j(\mathbf{x}_{source})$, to one of its unlike neighbors, $\mathbf{x}'_{target} \in \Omega'_{\mathbf{x}_{source}}$, also randomly selected. The net energy difference due to the proposed change of domain configuration, $\Delta H|_{j(\mathbf{x}_{source})\to j(\mathbf{x}_{target})} = H_{(after\ spin\ copy)} - H_{(before\ spin\ copy)}$, is then evaluated. The trial spin update is finally accepted with a Boltzmann-like probability function:

$$P(j(\mathbf{x}_{source}) \to j(\mathbf{x}_{target}))(t) = \tanh(\varepsilon T_{j(\mathbf{x}_{source})}(t)) \min\{1, e^{-\Delta H|_{j(\mathbf{x}_{source})\to j(\mathbf{x}_{target})}/T_{j(\mathbf{x}_{source})}(t)}\} \tag{2.1}$$

where $T_{j(\mathbf{x}_{source})}(t) \in \mathbb{R}^+$ is a Boltzmann temperature, a sort of agitation rate of moving compartment $j(\mathbf{x}_{source})$. The specific form of (2.1) is a modification of the classical probability function (recovered in the limit $\varepsilon \to \infty$) so that it is possible to treat the cases of frozen or of low motility individuals, for which the probability of moving is null or limited even in the presence of favorable energy gradients, as detailly commented in [62]. Specifically, given i the individual to which the moving compartment $j(\mathbf{x}_{source})$ belongs to, we set:

$$T_{j(\mathbf{x}_{source})}(t) = \begin{cases} T_N & \text{if} \quad \tau(j(\mathbf{x}_{source})) = N; \\ \\ T_0 \left[\dfrac{n^i(t)}{n_0^i + h\ (n^i(t) - n_0^i)} \right] & \text{if} \quad \tau(j(\mathbf{x}_{source})) = C. \end{cases} \tag{2.2}$$

Eq. (2.2) realistically differentiates between the low mobility of cell nucleus, which is passively dragged by the surrounding cytosolic region (see [61, 62] for comments), and the intrinsic motility of the overall cell, which is a measure of the agitation of its cytoskeleton (i.e., by the random actin polymerization/depolarization dynamics) and is assumed to be enhanced by the intracellular level of growth factors (i.e., motogen agents) in a dose-dependent manner. The quantity $n^i(t) = \sum_{\mathbf{x}\in i} n(\mathbf{x}, t)$ is in fact the total amount of growth factors inside cell i, as $n(\mathbf{x}, t)$ is their local concentration, defined in Eq. (2.7), while $n_0^i = \sum_{\mathbf{x}\in i} n_0$ is instead their overall basal level. T_0 therefore corresponds to the basal motility of tumor cells, while T_0/h is their asymptotic motility for saturating concentrations of chemicals. The above hypothesis are in agreement with experimental observations providing, through classical wound healing experiments, that high concentrations of growth factors stimulate the migratory capacity of different tumor cell lines (see for example [18, 19] for the Hepatocyte Growth Factor, [9, 69] for the Vascular Endothelial Growth Factor families, and [65] for the Fibroblast Growth Factor).

For any given time t the free energy, whose minimization, as seen, drives the system evolution, is:

$$H(t) = H_{shape}(t) + H_{adhesion}(t) + H_{haptotaxis}(t). \tag{2.3}$$

H_{shape} models the geometrical attributes of cell subunits. They are written as relative deformations in the following form:

$$H_{shape}(t) = H_{volume}(t) + H_{surface}(t) = \sum_{i,j} \left[\kappa_{i,j} \left(\frac{v_{i,j}(t) - V_{\tau(j)}}{v_{i,j}(t)} \right)^2 + \nu_{i,j} \left(\frac{s_{i,j}(t) - S_{\tau(j)}}{s_{i,j}(t)} \right)^2 \right], \tag{2.4}$$

where $v_{i,j}(t)$ and $s_{i,j}(t)$ represent actual volume and surface of the compartment j of cell i, and $V_{\tau(j)}$ and $S_{\tau(j)}$ the same quantities in the relaxed state, which correspond to their initial measures.

The formulation of (2.4) allows to have finite energetic contributions, as well as a blow up in the case of $v_{i,j}(t), s_{i,j}(t) \to 0$. This means that for instance an infinite energy is needed to shrink a cell to a point. $\kappa_{i,j}(t)$ and $\nu_{i,j}(t)$ are mechanical moduli in units of energy. In particular, $\kappa_{i,j}(t) \in \mathbb{R}^+$ refer to volume changes of the subcellular units, while $\nu_{i,j}(t) \in \mathbb{R}^+$ relate to their resistance to compression. Assuming that the cells do not significantly grow during invasion, the fluctuations of their volumes are kept negligible with high constant values of $\kappa_{i,j} = \kappa$, for any i and j. Moreover, because tumor cells are typically deformable, as they are able to significantly remodel to invade their surroundings more efficiently, for any i and for j such that $\tau(j) = C$ $\nu_{i,j} = \nu_C$ needs to be sufficiently low. The relative rigidity of the nucleus (with respect to the cytoplasm) is instead modeled by an high value of $\nu_{i,j} = \nu_N$, where $\tau(j) = N$.

$H_{adhesion}$ is the general extension of Steinberg's Differential Adhesion Hypothesis (DAH) [28, 66, 67]. In particular, it is differentiated in the contributions due to either the generalized contact tension between the nucleus and the cytosol belonging to the same cell, or to the effective adhesion between different cells or between a cell and the external environment, see also [62]:

$$H_{adhesion}(t) = H^{int}_{adhesion}(t) + H^{ext}_{adhesion}(t) = \sum_{\substack{\mathbf{x}\in\Omega, \mathbf{x}'\in\Omega'_{\mathbf{x}} \\ i(j(\mathbf{x}))\neq i(j(\mathbf{x}')) \\ j(\mathbf{x})\neq j(\mathbf{x}')}} J^{ext}_{\tau(j(\mathbf{x})),\tau(j(\mathbf{x}'))} + \sum_{\substack{\mathbf{x}\in\Omega, \mathbf{x}'\in\Omega'_{\mathbf{x}} \\ i(j(\mathbf{x}))=i(j(\mathbf{x}')) \\ j(\mathbf{x})\neq j(\mathbf{x}')}} J^{int}_{\tau(j(\mathbf{x})),\tau(j(\mathbf{x}'))}, \tag{2.5}$$

where the Js are binding energies per unit of area, which are obviously symmetric. In particular, the high negative value set for $J^{int}_{N,C}$ prevents cells from fragmenting (we refer to [50, 62] for comments). $J^{ext}_{C,C}$ represents instead the adhesive strength between the membranes of two nearby cells, a measure of the quantity of active and exposed cadherins. Finally, $J^{ext}_{C,M}$ evaluates the heterophilic adhesive bonds between the integrins on the cell surface and suitable ligands (such as laminin and fibronectin) in the extracellular matrix. By setting constant and homogeneous values for both $J^{ext}_{C,C}$ and $J^{ext}_{C,M}$, we assume a uniform distribution of adhesion molecules on the cell surface and a homogenous density of ligands in the external microenvironment. In particular, since malignant cells have been demonstrated to have reduced cell-cell adhesiveness but increased cell-ECM adhesiveness, due to a change in the relative expression of the corresponding adhesive molecules [32], we set $J^{ext}_{C,M} = 2\ J^{ext}_{C,C}$.

$H_{haptotaxis}$ reproduces the effect of cell preferential movement in the direction of zones with higher concentration of extracellular matrix proteins (such as fibrin, vitronectin, and some of the collagen family) and is implemented with a local linear-type relation:

$$\Delta H_{haptotaxis} = \mu \left[p_t(\mathbf{x}_{target}, t) - p_t(\mathbf{x}_{source}, t) \right], \tag{2.6}$$

where $\mathbf{x}_{source}$ and $\mathbf{x}_{target}$ are, respectively, the source and the final lattice site randomly selected during a trial update in a MCS, see (2.1), and $p_t(\mathbf{x}, t) = p(\mathbf{x}, t) + \sum_{\mathbf{x}'\in\Omega'_{\mathbf{x}}} p(\mathbf{x}', t)$, where $\mathbf{x} \in \{\mathbf{x}_{source}, \mathbf{x}_{target}\}$, evaluates the local level of ECM proteins sensed by the moving cell membrane site, as $p(\mathbf{x}, t)$ is their amount at site $\mathbf{x}$ (defined in Eq. (2.8)). Finally, $\mu \in \mathbb{R}^+$ represents the local strength of haptotaxis. The term (2.6) is similar to that used in [60] for the chemotactic processes in Dictyostelium Discoideum aggregation.

2.2. Continuous Model for Microenvironmental Variables

Available growth factors are supplied to the medium, diffuse and decay at a constant rate, and are consumed by tumor cells. Their spatial profile, $n(\mathbf{x},t)$, therefore satisfies the following equation:

$$\begin{aligned}\frac{\partial n(\mathbf{x},t)}{\partial t} = \underbrace{D_n\nabla^2 n(\mathbf{x},t)}_{diffusion} - \underbrace{\lambda_n n(\mathbf{x},t)\delta(\tau(j(\mathbf{x})),M)}_{decay} + \\ - \underbrace{\min\{n_{max},\chi_n n(\mathbf{x},t)\}(1-\delta(\tau(j(\mathbf{x})),M))}_{uptake} + \underbrace{S}_{production},\end{aligned} \tag{2.7}$$

where $\delta(\tau(j(\mathbf{x})),M)) = 1$ in the extracellular environment and 0 within cells. D_n is the characteristic diffusion coefficient, homogeneous throughout domain Ω and λ_n is the decay rate in the ECM. The third term in (2.7) models the local uptake by tumor cells, which follows a piecewise-linear approximation of a Michaelis-Menten law. In particular, $\chi_n \gg \lambda_n$, as we assume that the nutrient natural decay is negligible compared to the uptake by tumor cells. S describes the production of chemical factors at a constant rate ϕ_n per unit of time by a planar source, whose location and extension will be discussed in the next section.

The substrate contains matrix soluble proteins (i.e., we neglect their production, assuming a uniform distribution at the beginning of each simulation, see next section for more details), that naturally decay and that are degraded by the metalloproteinases (MMPs) secreted by malignant cells. The change in the local amount of ECM proteins, $p(\mathbf{x},t)$, is therefore described by:

$$\frac{\partial p(\mathbf{x},t)}{\partial t} = -\underbrace{\lambda_p p(\mathbf{x},t)}_{decay} - \underbrace{\chi_p p(\mathbf{x},t)m(\mathbf{x},t)}_{degradation}, \tag{2.8}$$

where λ_p and χ_p are, respectively, non-negative decay and degradation rates, constant within the entire simulated substrate. In particular, we assume $\lambda_p \ll \chi_p$ to indicate a much higher dissolution of ECM proteins due to the activity cell proteolytic enzymes than to the physiological decay. $m(\mathbf{x},t)$ is the concentration of tumor-secreted MMPs, which is governed by:

$$\frac{\partial m(\mathbf{x},t)}{\partial t} = \underbrace{D_m\nabla^2 m(\mathbf{x},t)}_{diffusion} - \underbrace{\lambda_m m(\mathbf{x},t)\delta(\tau(j(\mathbf{x})),M)}_{decay} + \underbrace{\pi_m(1-\delta(\tau(j(\mathbf{x})),M))}_{production}, \tag{2.9}$$

where λ_m is the decay rate in the ECM and D_m the diffusion coefficient, whose low value models the fact that proteolysis is strongly localized in the regions close to the cell membrane, in agreement with experimental evidence in [48]. π_m is the constant production rate of degrading enzymes, active at each cell site.

Parameter	Description	Model Value
V_N	volume of nuclear compartment	50 [μm^2]
S_N	surface of nuclear compartment	43 [μm]
V_C	volume of cytosolic compartment	150 [μm^2]
S_C	surface of cytosolic compartment	90 [μm]
T_N	generalized motility of the nucleus	1
T_0	basal motility of cancer cells	4.5
ε	coefficient of Boltzmann-like probability function	1
h	Michaelis-Menten coefficient for T	1/3
κ	volume compressibility	10
ν_C	cytoplasm elasticity	5
ν_N	nucleus elasticity	10
$J^{int}_{N,C}$	generalized adhesion between nucleus and cytosol	-20
$J^{ext}_{C,C}$	cell-cell adhesive strength	5
$J^{ext}_{C,M}$	cell-matrix adhesive strength	2.5
μ	haptotaxis strength	5
D_n	diffusion constant of nutrients	10^3 [μm^{2}s^{-1}]
λ_n	on-rate constant of nutrient decay	$2 \cdot 10^{-4}$ [s^{-1}]
χ_n	on-rate constant of nutrient uptake	1 [h^{-1}]
ϕ_n	on-rate constant of growth factor production	0.78 [h^{-1}]
n_{max}	maximal growth factor consumption	0.08 [pg/cell/h]
$n_{ext,0}$	initial extracellular level of growth factors	10 [μM]
n_0	basal intracellular level of growth factors	0.2 [μM]
λ_p	on-rate constant of ECM protein decay	$1.3 \cdot 10^{-4}$ [s^{-1}]
χ_p	on-rate constant of ECM protein degradation	3 [h^{-1}]
$p_{ext,0}$	initial extracellular level of ECM protein	4 [μM]
D_m	diffusion constant of MMPs	5^{-4} [μm^{2}s^{-1}]
λ_m	on-rate constant of MMP decay	$2 \cdot 10^{-3}$ [s^{-1}]
π_m	on-rate constant of MMP production	$5 \cdot 10^{-3}$ [s^{-1}]

3. Simulation Details

The simulation domain Ω is a square lattice of 500 $\times$ 500 sites. The characteristic length of each site is 2 μm, and therefore Ω has a physical size of 1 mm. One MCS is set to correspond to 20 sec: the overall simulations stop after 15000 MCS, so that they reproduce a time-lapse of nearly 4 days. The PDE for the evolution of nutrients is numerically solved with a finite difference scheme on a grid with the same spatial resolution as Ω, characterized by 30 diffusion steps per MCS. This temporal scale is sufficiently small to guarantee the stability of the numerical method.

As represented in Fig. 4, the initial conditions of all simulations consist of a layer of tumor cells, whose initial dimensions correspond to their target measures given in Table I. This configuration is consistent with a spatially extended cancer mass which is invading from an epithelial cell lining down its basement membrane into the surrounding stroma. The boundary conditions for both growth factors, n, and proteolytic enzymes, m, are periodic at the left and the right sides of the domain (i.e., at $x = 0$ and $x = 500$) and zero flux at the bottom (i.e., at $y = 0$). In particular, the lateral periodic conditions are set since the simulated malignant population is a section of a much larger lesion, that could not be reasonably modeled on our grid. The zero fluxes at $y = 0$ are set assuming that this part of the tissue is far enough from the front of the tumor mass. For the same reason, we set a no flux condition for the MMP field at the top of the domain (i.e., at $y = 500$). The upper border of the grid represents instead an extended, planar source for the environmental growth

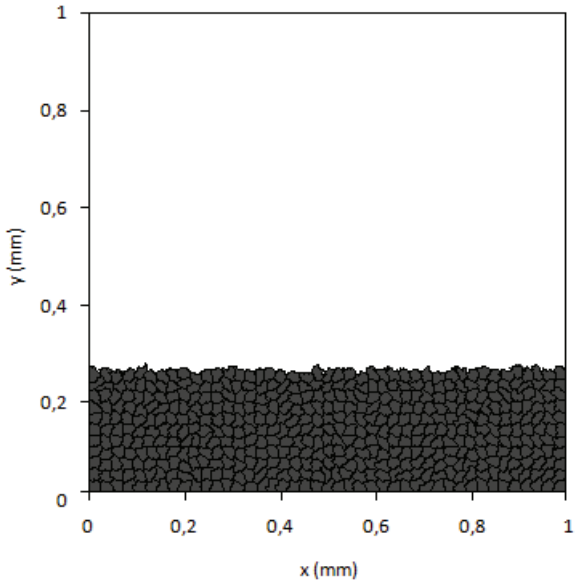

Figure 4: Initial condition (i.e., at t=0) of the tumor mass for all sets of simulations. The dimensions of cells, as well as all the other model parameters, are given in Table I.

factors, which are supplied by the host stroma throughout the basement membrane: consequently, we set $n((x, y = 500), t) = \phi_n$.

The parameter describing the biophysical properties of the cells, such as their basal motility, elasticity and adhesive strengths, have been evaluated, consistently with biological considerations clarified along the text, through preliminary simulations, that showed the model consistency in a wide range of values. This leads to confidence in the biological relevance of the results, which have been also confirmed by empirical comparisons with their experimental counterparts. The intracellular basal level of chemical factors, n_0, is instead sufficiently high to avoid that cells irreversibly enter the apoptotic state. The extracellular environment is initially seeded with a saturating level of proteins, $p_{ext,0}$, while there are no secreted MMPs in the extracellular medium.

To quantify the effects of the different model parameters on the tumor phenotype, we concentrate on the final depth of invasion of the mass at the end of the simulations (i.e., at t= 15000 MCS $\approx$ 4 days), given by:

$$d_f = \frac{1}{N} \sum_{i=1}^{N} (d_i - d_0) \,, \tag{3.1}$$

where d_i represents the final distance between a tumor cell and the bottom border of the domain and d_0 is the initial width of malignant mass. The average of $N = 10$ randomly chosen values is used to avoid biases towards accounting for outlier individuals. d_f has a clear clinical relevance, since it quantitatively estimates the severity of the disease and characterized the presence of metastasis delocalized with respect to the main body of the tumor.

4. Results

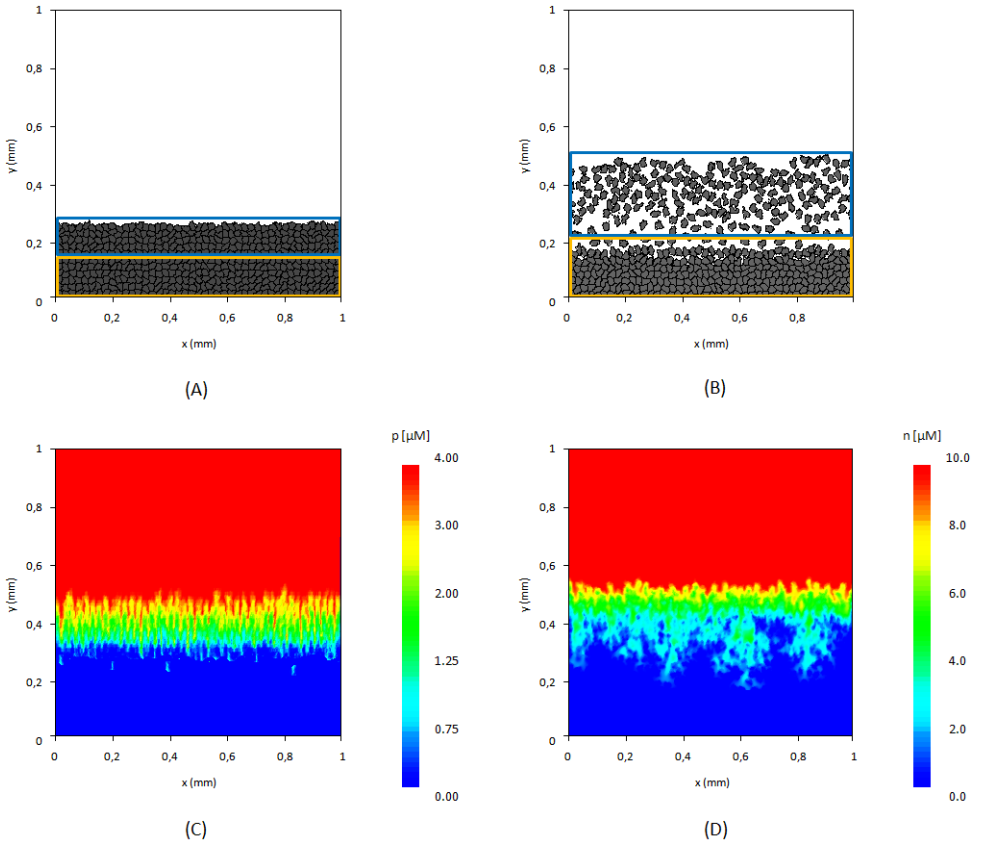

Figure 5: Invasion of the tumor mass and relative modification of the microenvironment with the standard parameter setting, given in Table I. (A) Color-coded regions in which the tumor mass is divided form its front, i.e. external and internal. (B) Configuration at t= 15000 MCS $\approx$ 4 days. (C) ECM protein distribution and (D) growth factor concentration in the host tissue at the end of malignant invasion (i.e., at t= 15000 MCS $\approx$ 4 days).

We first simulate the evolution of the tumor with the standard parameter setting. The malignant mass is observed to have an overall movement biased toward the extracellular environment, which is significantly invaded, as $d_f \approx 200$ μm, see Fig. 5(B). Consistently with the experimental evidences provided in the Introduction (see also Fig. 1), the invasive phenotype is largely mediated by the aggressive behavior of the more "external" cells (i.e., those placed near the front of the mass, see blue color-coded region in Fig. 5(A)), which loosen contacts, dissociate, move from their original site and start wandering in the close proximity, displaying an evident ability to spread in the surrounding tissue. The increased metabolism of these individuals is due to the availability of growth factors which, together with the interactions with the local microenvironment (both the haptotactic movement and adhesive preference for ECM components) induces a sort of mesenchymal transition able to overcome the physiological regulation of the mechanism of contact-inhibition of

cell locomotion (firstly proposed by Abercrombie to describe the influence on cell crawling of the contact interactions between individuals [1]). The rest of the population remains instead relatively compact, with only some cells wade just outside the body of the tumor, see yellow-coded region in panels (A) and (B) of Fig. 5. The migratory and invasive capacity of such "internal" individuals is in fact inhibited by both the limited access to chemicals and by the high cellular density, which enforce cell-cell adhesive interactions. As shown in Fig. 5(C-D), at the end of the invasive phase, the host tissue is significantly modified, as the matrix proteins have been dramatically degraded (notice in the same figure the paths of protein gradients which drive cell migration) and the growth factors have been significantly consumed.

As briefly sketched in Sec. 2, the values of the parameters J^{ext}s have a clear biological relevance, as they describe the relative preference of tumor cells to be in contact with other cells or with the extracellular medium. At a molecular level, they are therefore a measure of the expression and the engagement of the different types of cell adhesion molecules, cadherins and integrins, respectively. Indeed, the variation of the J^{ext}s is expected to have a substantial impact on the overall invasiveness of the disease. We first change the cell-cell adhesive strength $J^{ext}_{C,C}$, see Fig. 6. At low values of the parameter (i.e., $J^{ext}_{C,C} < J^{ext}_{C,M}$, which means higher cell-cell adhesiveness), the tumor remains compact, with the highly motile external cells that clump along the front of the mass, rather than invading significantly the surrounding tissue, see Fig. 6(A). This phenomenology is due to the fact that the cell-cell adhesive interactions are too strong to be overcome by the other forces experienced by malignant individuals and therefore stabilize tumor morphology. At large values of $J^{ext}_{C,C}$, the tumor instead expands and invades deeper: the external cells quickly spread away from the rest of the mass creating a dispersed front (fewer of them are in contact with each other within 12 hours) and a repulsion occurs also among individuals within the main body of the mass. The subsequent formation of islands of free matrix within the center of the tumor, which are then only partially filled in again, increases the overall bias toward invasion, as reproduced in Fig. 6(B). From these results, we can confirm that an alteration in cell-cell adhesive properties is an important consideration in determining the severity of the disease. In particular, a biomedical intervention that is able to enforce cell-cell adhesive interactions allows to control the morphology of the lesion which, remaining smooth and densely packed, can be more easily treated surgically. The presented computational outcomes are consistent with a number of *in vitro* experiments: for example glioma cell lines with a high N-cadherin expression have been seen to invade less significantly different types of collagenous matrices [30]. We next vary $J^{ext}_{C,M}$. The decrement of $J^{ext}_{C,M}$ has a relatively subtle effect on the malignancy of the tumor, as its invasive distance does not dramatically change, see Fig. 7(B). This is due to the fact that tumor cells prefer to adhere to extracellular matrix elements already with the standard parameter setting, (i.e., $J^{ext}_{C,M} < J^{ext}_{C,C}$, see Table I). At high values of $J^{ext}_{C,M}$ (i.e., $J^{ext}_{C,M} > J^{ext}_{C,C}$, which means a lower cell-matrix adhesiveness) the invasion is instead strongly discouraged, as also the cells at the front remain close to the body of the mass, with occasional individuals shed in the extracellular environment, see Fig. 7(A). The cancerous cells are in fact simulated to have an underexpression of integrin molecules: the haptotactic force alone is unable to balance the cell-cell adhesive interactions and therefore to cause the scatter of individuals. These considerations suggest that the use of drugs that interfere with cell-matrix adhesive interactions, either by altering the amount of ligand in the matrix or by

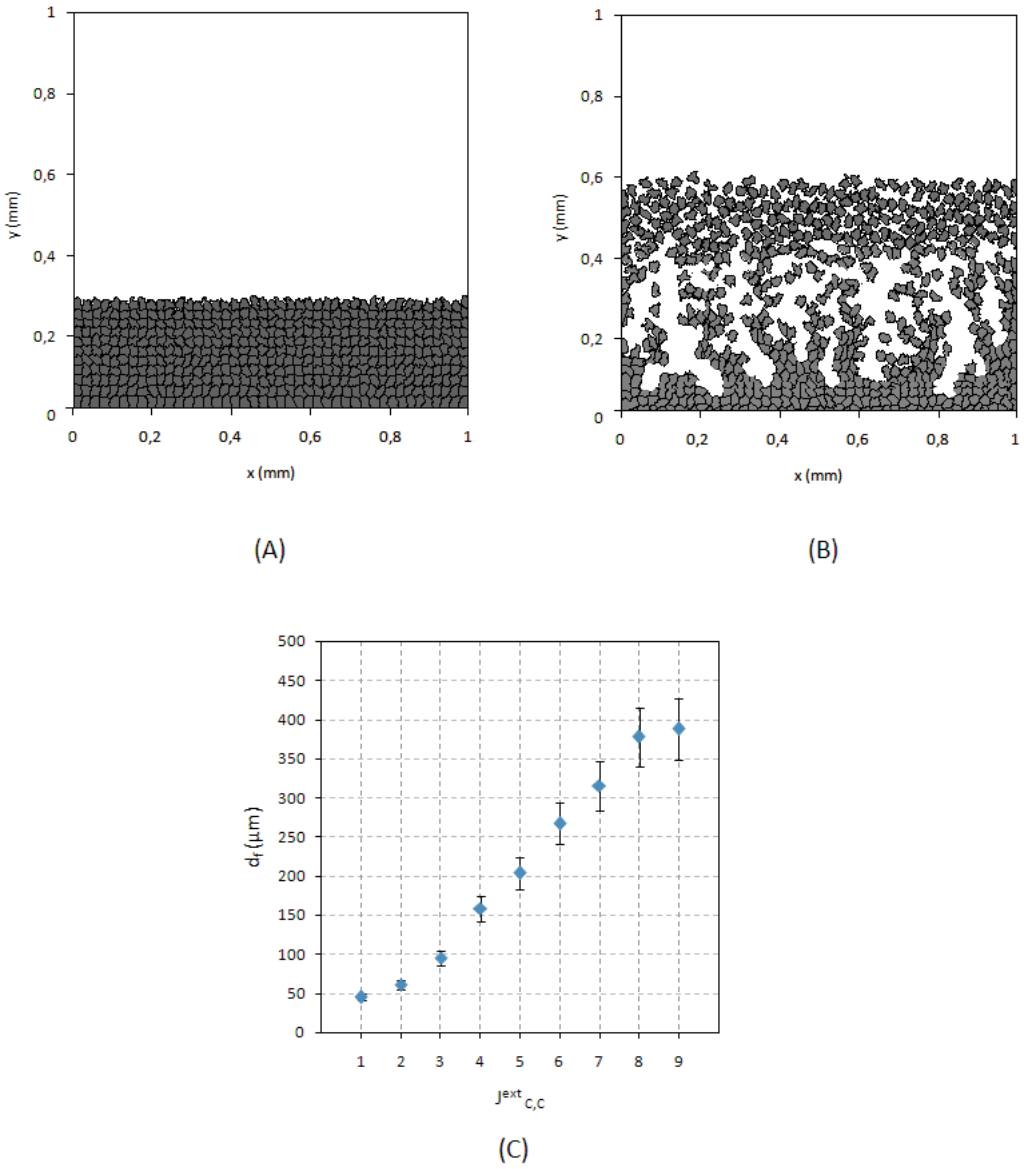

Figure 6: Invasiveness of the tumor mass in response to alterations of cell-cell adhesive strength, $J^{ext}_{C,C}$ (i.e., all the other model parameters are the same as in the simulation in Fig. 5). Decrements in cell-cell adhesion lead to increments in the malignancy of the lesion. On the contrary, by enforcing cell-cell adhesion, the mass remains compact and smooth with a low invasive potential. Examples of final configurations for (A) $J^{ext}_{C,C} = 1$ and (B) $J^{ext}_{C,C} = 8$. In this last case, it is possible to see islands of free matrix formed in the main body of the mass, as repulsion occurs also among internal individuals. (C) Final depth of invasion d_f vs $J^{ext}_{C,C}$, error bars show standard deviation over 10 realizations.

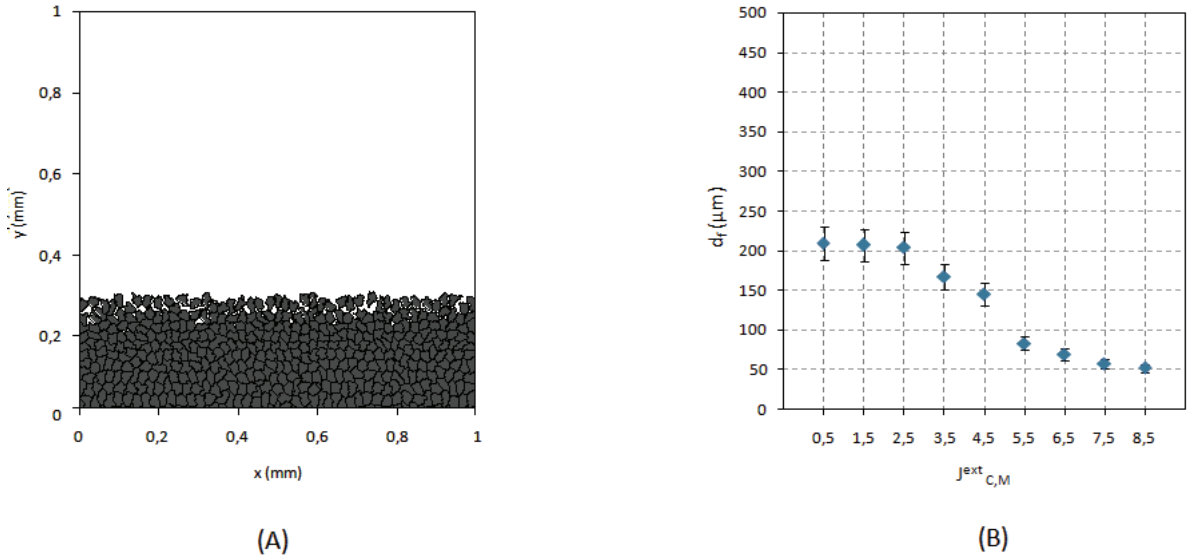

Figure 7: Invasiveness of the tumor mass in response to alterations of cell-matrix adhesive strength, $J^{ext}_{C,M}$ (i.e., all the other model parameters are the same as the simulation in Fig. 5). Decrements in cell-matrix adhesive interactions discourage the aggressive behavior of the lesion. In particular, for high $J^{ext}_{C,M} > J^{ext}_{C,C}$, the malignant cells remain closely packed each other. (A) Final configuration for $J^{ext}_{C,M} = 8.5$. (B) Final depth of invasion d_f vs $J^{ext}_{C,M}$, error bars show standard deviation over 10 realizations.

inhibiting integrin molecules (which, as seen, are overexpressed in tumors), has the potential to limit malignant invasion, and eventually, to render the cancer more partial to resection.

We now turn to address how the invasiveness of the tumor changes as a function of ν_C, that describes the degree of cell membrane elasticity, see Fig. 8. Small values of ν_C allow the cells to reorganize their shape more substantially and to traverse the extracellular matrix more readily. The consequent enhancement of invasiveness is due to a distribution of the external individuals, which, able to remodel their shape to adapt to the directions of ECM protein gradients, can venture further from the main body of the mass, as reproduced in Fig. 8(A). At high values of ν_C, a decrement of the invasive distance instead occurs, as the malignant cells cannot reorganize and expand efficiently in their environment, even if they have an increased motility and the preference to heterophilic (i.e., cell-matrix) contacts, see Fig. 8(B). Indeed, we can conclude that the ability of tumor cells to undergo continuous and dramatic changes in their morphology during motion has a big impact on the aggressiveness of the disease, as also provided in [58]. A therapeutic approach that targets the dynamics of polarization/depolarization of the cytoskeletal of cancer cells, as the use of phalloidin-like compounds, may be therefore potentially effective.

We finally analyze how the invasiveness of the tumor is influenced by the haptotactic capacity related to the coefficient μ, see Fig. 9(A). An increased sensitivity of cells to ECM protein gradients prompts in fact the tumor front to more significantly move in the extracellular environment, eventually promoting invasion. On the contrary, low values of μ results in an isotropic movement of malignant individuals, which are therefore unable to maintain directional persistence and

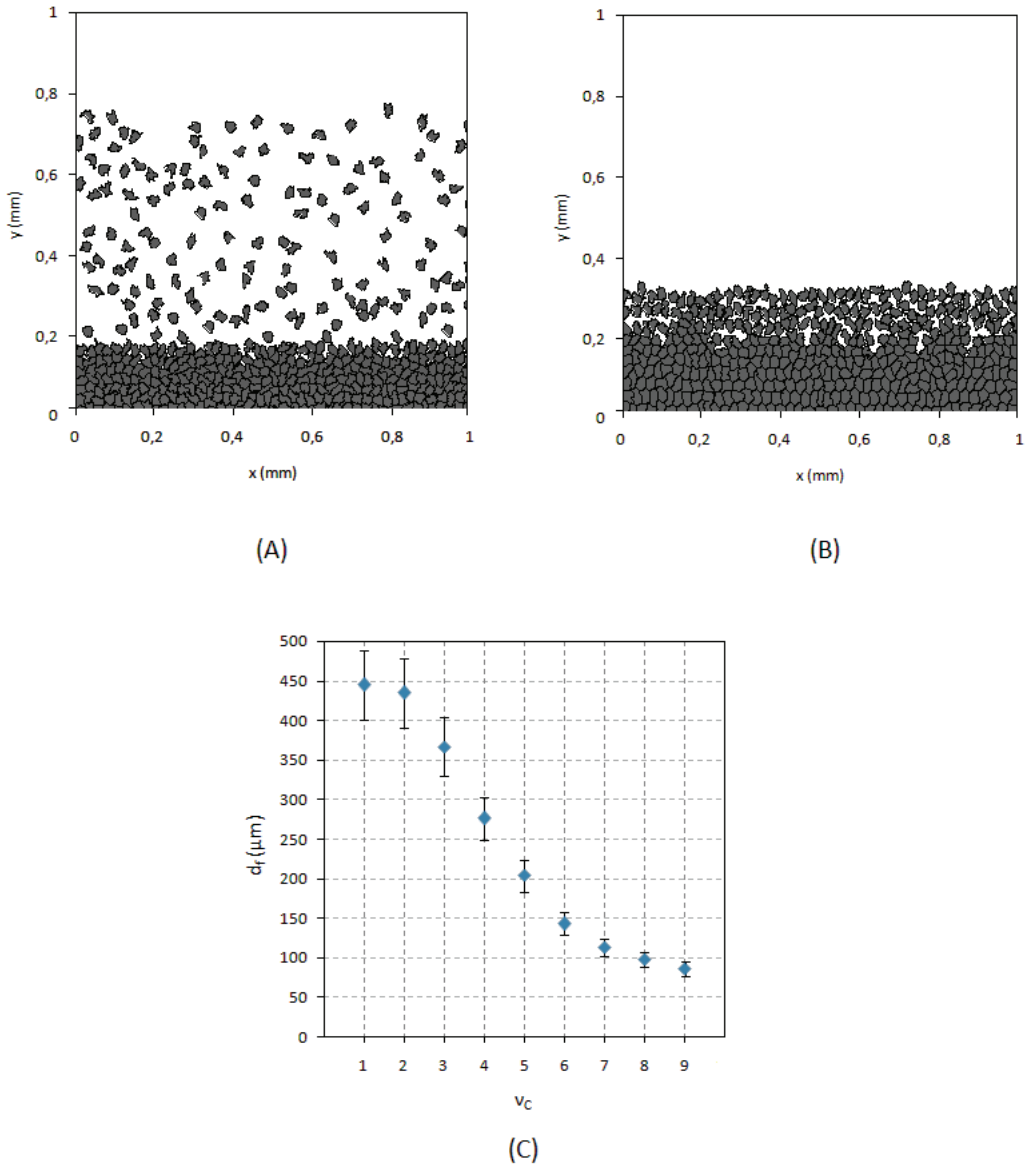

Figure 8: Invasiveness of the tumor mass in response to alterations in cell membrane elasticity, ν_C (i.e., all the other model parameters are the same as in the simulation in Fig. 5). Increments in cell ability to remodel cause dramatic increment in malignant aggressiveness, as the cells can efficiently traverse the host tissue. On the contrary, if cells are forced to maintain their shape, they behave as rigid bodies and do not venture far from the front of the main mass. Examples of final configurations for (A) $\nu_C = 1$ and (B) $\nu_C = 8$. (C) Final depth of invasion d_f vs ν_C, error bars show standard deviation over 10 realizations.

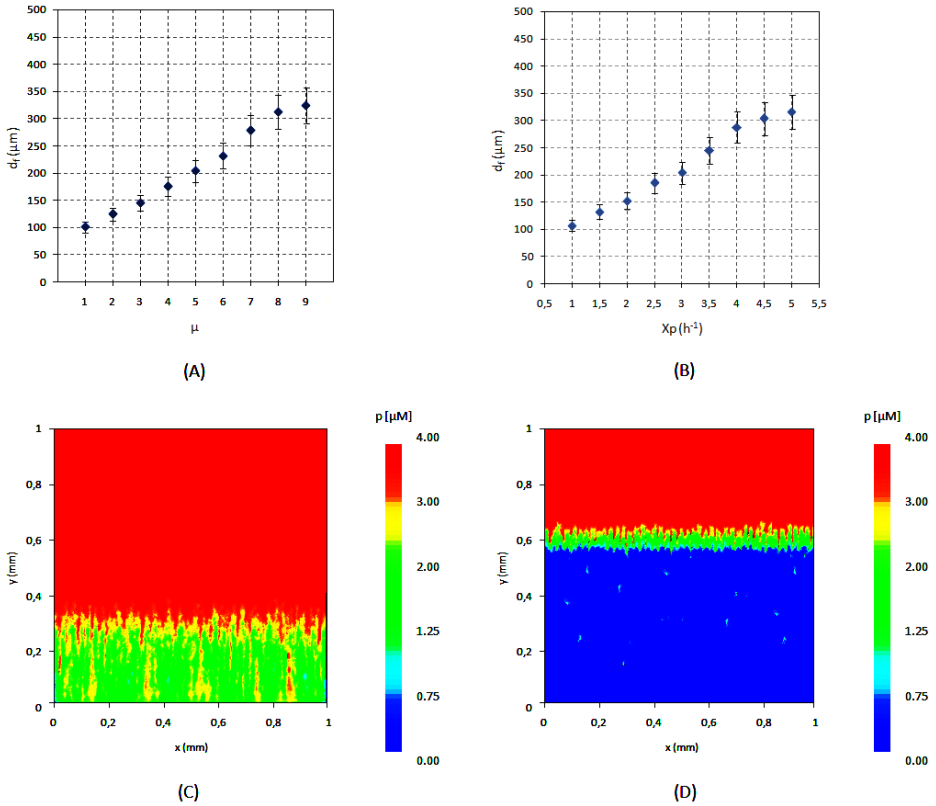

Figure 9: Invasiveness of the tumor mass in response to alterations in the interactions between malignant cells and ECM substrate. (A) Final depth of invasion d_f vs haptotactic coefficient μ (all the other model parameters are the same as in the simulation in Fig. 5), error bars show standard deviation over 10 realizations. Inhibitions of cell sensitivity translate in decrements of the aggressiveness of the lesion. (B) Final depth of invasion d_f vs degradation rate of ECM proteins χ_p (all the other model parameters are the same as in the simulation in Fig. 5), error bars show standard deviation over 10 realizations. A downregulation of the activity of tumor MMPs results in a more homogeneous pattern of protein distribution: therefore malignant individuals have not a directional path to follow during their motion. Final pattern of ECM protein concentration for (C) $\chi_p = 1$ and (D) $\chi_p = 5$. In the last images, we do not explicitly represent the cell configuration: however the invasive deep of the shed malignant individuals is easily recognized by looking the interface between the zones with partially degraded matrix components and those with the initial amount of substrate.

to deeply penetrate in the host tissue. The inhibition of cell haptotactic sensitivity can therefore represent a potential efficient intervention strategy. In particular, it can be reproduced *in vitro* by adding saturating amounts of matrix components, that extinguish substrate inhomogeneities. At this regard, experimental evidence have demonstrated that, consistently with our results, cells cultured in matrices with high collagen densities show a dramatic downregulation of their migratory capacity, driven by the fact that their integrin receptors are completely engaged without maximal cell spreading and movement [20, 22]. An analogous behavior is seen by varying the cell proteolytic activity, measured by the parameter χ_p, see Fig. 9(B). In particular, low values of χ_p translate into a partial degradation of ECM proteins, see Fig. 9(C), whose pattern remains almost homogeneous and significantly inhibits the haptotactic component of the migration of cancer cells (that is fundamental for tumor aggressiveness). High values of χ_p result instead in a dramatic digestion of the matrix substrate and in the consequent formation of steep gradients, as reproduced in Fig. 9(D), which enhance the directional movement of malignant individuals, eventually causing an unstable and dispersed morphology of the tumor. The scattered cells at the front of the mass in fact deeply penetrate into the host tissue to reach regions with sufficient amounts of ECM proteins. These observations agree with the correlation experimentally found between the malignancy and the metastatization ability of most tumors and the activity of the secreted matrix metalloproteinasis, see for example [35].

5. Cell Proliferation

So far, we have correlated the invasive phenotype of a solid tumor with the biophysical properties of mutated cells, and with their interactions with the local microenvironment. However, malignant individuals are seen to have also a higher proliferation rate than to their unmutated counterparts. In particular, as suggested by a number of experimental works as early as [63], the time between cell divisions has a stochastic distribution, which depends on both the internal state of each cell and on the time from its last mitotic process (i.e., except for extremely rapidly dividing cells, those who recently divided will be still growing and the likelihood of their reentering the S phase is extremely small, see [3]). For each cell i, we therefore define its present probability P^i to undergo mitosis with the following functional form, which resembles that used in a similar approach [71]:

$$P^i(t) = \begin{cases} 0 & \text{if} \quad (t - t^i) \leq t_0; \\ \dfrac{n^i(t) - n_0^i}{n^i(t)} \dfrac{(t - t^i)^2}{(t - t^i)^2 + 1} & \text{if} \quad (t - t^i) > t_0. \end{cases} \tag{5.1}$$

t^i is the last time that cell i underwent mitosis, while t_0 is a dormant period during which the cells are prohibited to proliferate (i.e., it correspond to the G1 phase, during which the cells are metabolically active and grow). t_0 is set equal to 1300 MCS (i.e., ≈ 7 hours): since the mitotic rate varies greatly from tissue to tissue, and between different types of malignancies, this choice represents a compromise between very slow growing and very aggressive tumor types. Relation (5.1) takes into

account that, once the time since last division exceeds t_0, the probability of another mitosis slowly increases, and approaches 1 as it becomes very long. Moreover, a cell needs a sufficient quantity of growth factors to proliferate, as widely demonstrated in literature with mitogenic assays (refer for example to [46, 65, 73]) and explained in details in [3]. Procedurally, the mechanism of cell division is implemented by dividing the proliferating individual into two identical daughter cells, with both the nucleus (which is randomly located) and the cytosolic region halved with respect to their parent, see Fig. 10: however, due to the shape constraints in Eq. (2.4), they will gradually "maturate" into full-size cells. We further assume that both daughter cells evenly inherit all the parent's biophysical properties (i.e., its motility and adhesive properties). Finally, the newly formed individuals are placed symmetrically about the parent cell center of mass with a random orientation.

Intuitively, cell proliferation is expected to be dramatically proinvasive, on the basis that an increment in the cell population will facilitate the invasion of the extracellular environment. However, tumor invasiveness only slightly increases, as $d_f \approx 260$ μm, see Fig. 10. The explanation of this counter-intuitive result is that the external cells, whose metabolism is accelerated by the high quantity of available nutrients, quickly divide, forming a front of little islands, as reproduced in Fig. 10(B). Such cell clusters go on increasing in size, due to further cell proliferations, and come in contact with the main tumor mass by short and thick (4-5 cell-wide) "fingers", see Fig. 10(C). The increased cellular density, in turn, enforces cell-cell adhesive interactions, which balance the effect of the haptotaxis and of the enhanced cell motility. The formed fingers therefore do not break and, consequently, the overall invasion is partially discouraged. The phenomenon of "fingering" has been captured by other discrete models [64, 71], and characterizes many malignancies, see for example Fig. 10(E). In particular, recent studies of photo-micrograph have shown that the "ragged" surfaces of different tumors contains fractal components at the smaller, cellular scale, that relate to the overall severity of the disease [17, 36]. However, tumors with an unstable fingered morphology are typically more aggressive and hard to be treated than smoother ones: in fact, even if their invasive depth is limited, they are difficult to be surgically removed.

We finally characterize the tumor patterns emerging for different cell-cell adhesive interactions (i.e., given by parameter $J^{ext}_{C,C}$) in the case of either non-proliferative or proliferative individuals. The obtained results are graphically summarized in Figure 11. At high intercellular adhesiveness, the cancerous mass remains compact and smooth: indeed, its invasive distance is specifically determined by the mitotic rate of malignant individuals. On the opposite, at low cell-cell adhesion, the tumor invades the surrounding environments with a front of dispersed aggressive individuals, with islands of free tissue forming within the main mass. Also in this case, cell replication enhances the invasive potential of the cancer, leading to the most aggressive disease, which deeply penetrates in the surrounding tissue with an increasing number of scattered individuals. Finally, at intermediate values of intercellular adhesive connections, we observe the formation of a ragged tumor front only in the case of proliferative individuals: this suggests that fingers of malignant cells can emerge only with a specific balance between their mitotic potential and their adhesive strength. Reviewing the results in Fig. 11, we can therefore conclude that tumor patters are primarily differentiated by the variation of the cell adhesive potential, while the invasive depth is definitively dependent from the cell mitotic rate. Of particular interest is the unstable fingered morphology characterizing a small

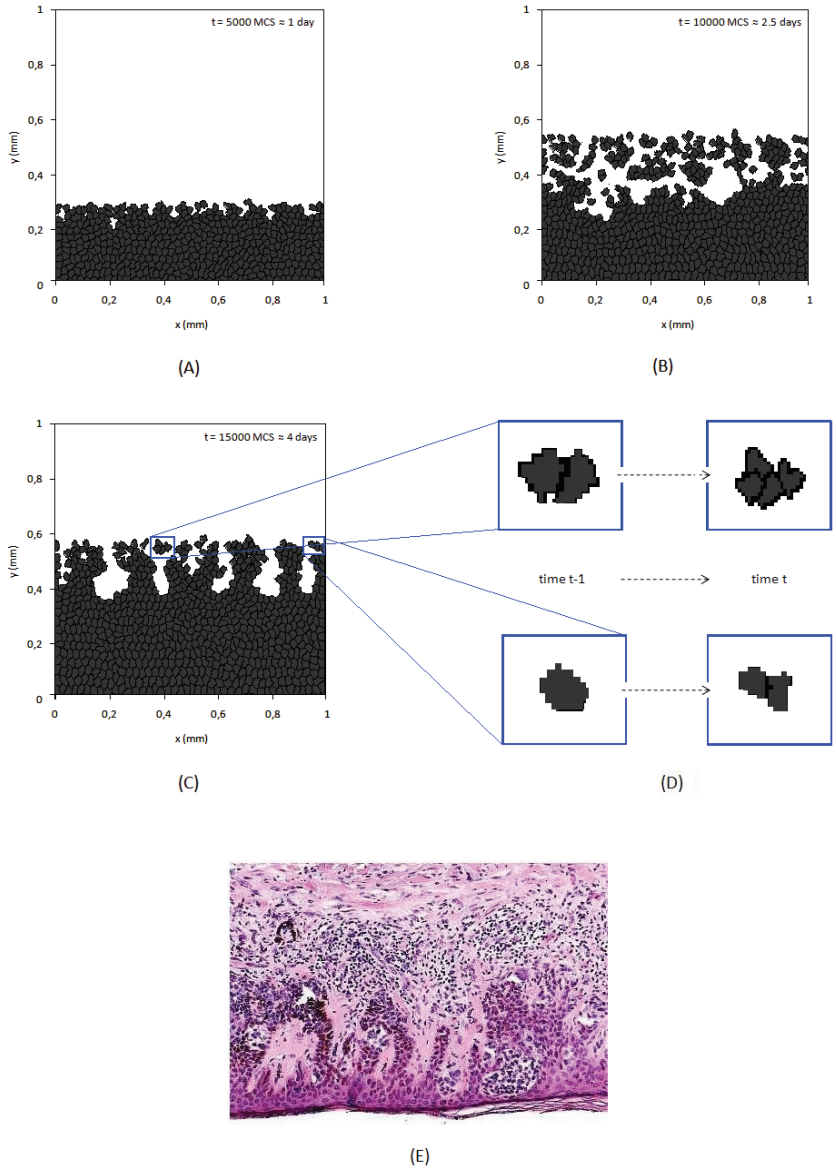

Figure 10: Tumor development with the inclusion of cell proliferation. External individuals quickly undergo mitosis, constituting a front of little islands, panel (B), which, due to further cell proliferations, come in contact with the main tumor mass by short and thick (4-5 cell-wide) "fingers", panel (C). The high cellular density, in turn, enforces cell-cell adhesive interactions, which balance the effect of the haptotaxis and the increased cell motility, and do not permit the brokage of the formed fingers. In the zoom views in panel (D), we show the division of three individuals, with the consequent formation of the daughter cells. (E) For comparison purpose, high-power photomicrograph of a lentiginous and junctional moderate melanocytic dysplasia in the epidermis overlying the dermal component. The papillary dermis is widened by a mixture of tumor cells, inflammatory cells, and fibrous tissue. At the bottom of the image, invading fronts of the neoplasm feature tentacular or finger-like extensions, similar to those reproduce by the computational model. Image courtesy of the Institute for Cancer Research and Treatment of Candiolo (I.R.C.C.).

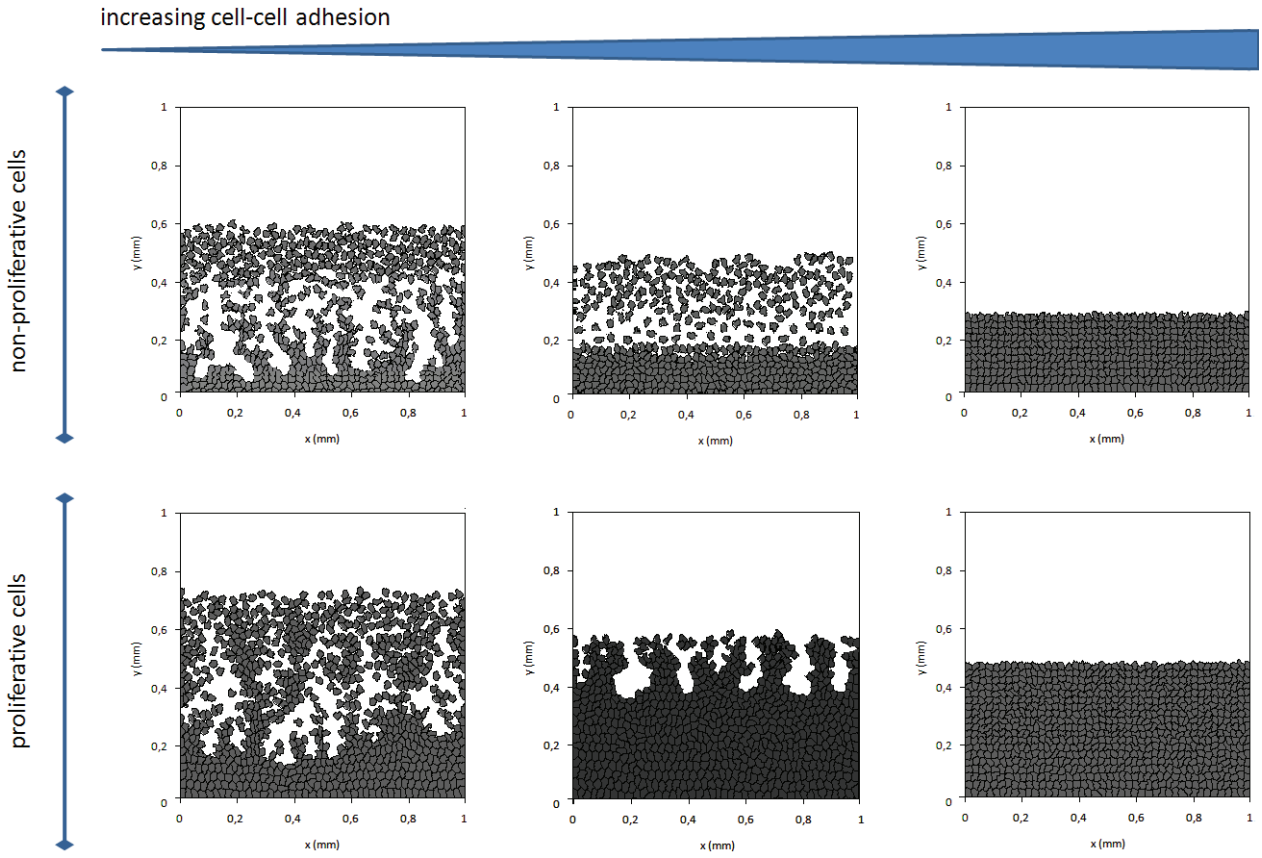

Figure 11: Resulting morphologies of the microinvasive tumor mass for different intercellular adhesive interactions (i.e., given by parameter $J^{ext}_{C,C}$) in the case of either un-proliferative or proliferative malignant individuals.

region of the cell biophysical parameter space.

6. Discussion

Solid tumor invasion is driven by the complex interplay of molecular- and cellular-scale dynamics of genetically damaged cells, that are able to survive and evolve even under extreme conditions, e.g. hypoxia and acidosis [21]. In particular, the invasiveness of a cancer mass can be a quantifiable function of the altered biophysical characteristic of malignant cells, such as their enhanced motility and metabolism and the downregulation in their cell-cell adhesion, as well as of their aggressive interactions with the local microenvironment, such as the enhanced consumption of available nutrients and degradation of ECM proteins. Accordingly, we here proposed a theoretical approach able to analyze the morphology of the lesion under different conditions and to quantify its malignancy and to predict the effects of therapeutic interventions specifically altering some of these component mechanisms. The computational framework is a hybrid composite environment, that used a discrete CPM to reproduce single cancer cells and a continuous approach to represent components of the tumor microenvironment, i.e. the transport and consumption of growth factors and the digestion of ECM protein by tumor-secreted MMPs.

Our results were primarily focused on biomedical strategies able to enforce a compact and non-invasive morphology of the tumor, so that the lesion could in principle be more easily resectable. In particular, in the light of the model outcomes, therapeutic interventions aiming at modulating the adhesive properties of tumor cells could result efficient. Such biomedical strategies should concentrate on strengthening cell-cell adhesion while inhibiting cell-matrix adhesion: in this way the malignant mass will remain compact and smooth and therefore would be easier to be surgically treated. Interventions that down-regulate the ability of tumor cells to either efficiently remodel and or to secrete MMPs could be also potentially efficient (for instance, the inhibition of MMP production has been demonstrated to be insufficient to decrease the overall malignancy of the disease, see [57]). Finally, we showed that the inclusion of cell proliferation (which has been explicitly related to the intracellular amount of growth factors) resulted in a change in the morphology of the invading mass, with the formation of short and thick "fingers" of cells. However, from the computational outcomes, the increment in cell density does not seem to lead to a significant increment in the invasive phenotype.

As explained, the proposed therapeutic strategies influence tumor invasiveness by directly affecting the actual biophysical properties of cancer cells. However, as briefly sketched, the phenotypes of malignant individuals typically origin from genetic or epigenetic mutations: therefore, with such biomedical treatments, we could not in principle exclude the recurrence of the disease. Indeed a fundamental improvement of our approach would consist in the introduction of the genetic level. This could in fact allow to explore quantitative links between genotypic abnormalities and altered behaviors of malignant individuals and to study the ultimate efficiency of the proposed therapies. Finally, the study of the tumor responses to the proposed therapies has to be eventually

translated into *in vitro* investigations that can reveal possible un-expected side effects.

Acknowledgements

Partially funded by the Italian Ministry of University and Research under a grant on "Math Models of the Interactions between Cells and Environment" and by Fondazione Credito di Risparmio di Torino (CRT) through a "Lagrange Project Fellowship".

References

[1] M. Abercrombie. *The crawling movement of cells.* Proc. R. Soc. London B., 207 (1980), 129 - 147.

[2] T. Alarcon, H. Byrne, P. Maini. *A cellular automaton model for tumour growth in inhomogeneous environment.* J. Theor. Biol., 225 (2003), 257 - 274.

[3] B. Alberts, A. Johnson, J. Lewis, M. Raff, K. Roberts, P. Walter. Molecular Biology of the Cell, 4th ed. Garland Science, New York, 2002.

[4] A. Anderson, A. Weaver, P. Commmings, V. Quaranta. *Tumor morphology and phenotypic evolution driven by selective pressure from the microenvironment.* Cell, 127 (2006), 905 - 915.

[5] A. Anderson. *A hybrid mathematical model of solid tumour invasion: the importance of cell adhesion.* Math. Med. Biol., 22 (2005), 163 - 186.

[6] R. Araujo, D. McElwain. *A history of the study of solid tumour growth: the contribution of mathematical modelling.* Bull. Math. Biol., 66 (2004), 1039- 1091.

[7] A. Balter, R. M. H. Merks, N. J. Poplawski, M. Swat, J. A. Glazier. *The Glazier-Graner-Hogeweg model: extensions, future directions, and opportunities for further study.* In A. R. A. Anderson, M. A. J. Chaplain, and K. A. Rejniak editors, Single-Cell-Based Models in Biology and Medicine, Mathematics and Biosciences in Interactions, Birkaüser, 151 - 167, 2007.

[8] N. Bellomo, N. K. Li, P. K. Maini. *On the foundations of cancer modelling: selected topics, speculations, and perspectives.* Math. Models Methods Appl. Sci., 18 (2008), 593 - 646.

[9] J. M. Bock, L. L. Sinclair, N. S. Bedford, R. E. Jackson, J. H. Lee, D. K. Trask. *Modulation of cellular invasion by VEGF-C expression in squamous cell carcinoma of the head and neck.* Arch. Otolaryngol. Head. Neck. Surg., 134 (2008), No. 4, 355 – 362.

[10] J. M. Brown. *Tumor microenvironment and the response to anticancer therapy.* Cancer Biol. Ther., 1 (2002), 453 - 458.

[11] A. Bru, S. Albertos, J. L. Subiza, J. L. Garca-Asenjo, I. Bru. *The universal dynamics of tumor growth.* Bioph. J., 85 (2003), No. 5, 2948 – 2961.

[12] Cancer modeling and simulation, L. Preziosi editor, Mathematical Biology and Medicine Sciences, Chapman and Hall/CRC, 2003.

[13] H. Byrne, T. Alarcon, M. Owen, S. Webb, P. Maini. *Modeling aspects of cancer dynamics: a review.* Philos. Trans. R. Soc. A., 364 (2006), 1563 - 1578.

[14] M. A. J. Chaplain, A. R. A. Anderson. *Mathematical modelling of tissue invasion.* In L. Preziosi editor, Cancer Modelling and Simulation, Chapman Hall/CRC, 269 – 297, 2003.

[15] V. Cristini, H. Frieboes, R. Gatenby, S. Caserta, M. Ferrari, J. Sinek. *Morphologic instability and cancer invasion.* Clin. Cancer Res., 11 (2005), 6772 - 6779.

[16] V. Cristini, J. Lowengrub, Q. Nie. *Nonlinear simulation of tumor growth.* J. Math. Biol., 46 (2003), 191 - 224.

[17] S. S. Cross. *Fractals in pathology.* J. Pathol., 182 (1997), 1 - 8.

[18] A. De Luca, N. Arena, L. M. Sena, E. Medico. *Met overexpression confers HGF-dependent invasive phenotype to human thyroid carcinoma cells in vitro.* J. Cell Physiol., 180 (1999), 365 – 371.

[19] M. F. Di Renzo, M. Oliviero, R. P. Narsimhan, S. Bretti, S. Giordano, E. Medico, P. Gaglia, P. Zara, P. M. Comoglio. *Expression of the Met/HGF receptor in normal and neoplastic human tissues.* Oncogene, 6 (1991), 1997 – 2003.

[20] A. Engler, L. Bacakova, C. Newman, A. Hategan, M. Griffin, D. Discher. *Substrate compliance versus ligand density in cell on gel responses.* Biophys. J., 86 (2004), 617 - 628.

[21] R. Gatenby, K. Smallbone, P. Maini, F. Rose, J. Averill, R. Nagle, L. Worrall, R. Gillies. *Cellular adaptations to hypoxia and acidosis during somatic evolution of breast cancer.* Br. J. Cancer, 97 (2007), 646- 653.

[22] C. Gaudet, W. Marganski, S. Kim, C. T. Brown, V. Gunderia, M. Dembo, J. Wong. *Influence of type I collagen surface density on fibroblast spreading, motility, and contractility.* Biophys. J., 85 (2003), 3329 - 3335.

[23] P. Gerlee, A. Anderson. *An evolutionary hybrid cellular automaton model of solid tumor growth.* J. Theor. Biol., 246 (2007), 583 - 603.

[24] P. Gerlee, A. Anderson. *Stability analysis of a hybrid cellular automaton model of cell colony growth.* Phys. Rev. E, 75 (2007), 051911.

[25] C. Giverso, M. Scianna, L. Preziosi, N. Lo Buono, A. Funaro. *Individual cell-based model for in-vitro mesothelial invasion of ovarian cancer.* Math. Model. Nat. Phenom., 5 (2010), No. 1, 203 – 223.

[26] J. A. Glazier, A. Balter, N. J. Poplawski. *Magnetization to morphogenesis: A brief history of the Glazier-Graner-Hogeweg model.* In A. R. A. Anderson, M. A. J. Chaplain, and K. A. Rejniak editors, Single-Cell-Based Models in Biology and Medicine, Mathematics and Biosciences in Interactions, Birkaüser, 79 - 106, 2007.

[27] J. A. Glazier, F. Graner. *Simulation of the differential adhesion driven rearrangement of biological cells*. Physical. Rev. E, 47 (1993), 2128 - 2154.

[28] F. Graner, J. A. Glazier. *Simulation of biological cell sorting using a two dimensional extended Potts model.* Phys. Rev. Lett., 69 (1992), 2013 - 2017.

[29] H. Hatzikirou, A. Deutsch, C. Schaller, M. Simon, K. Swanson. *Mathematical modeling of glioblastoma tumour development: a review.* Math. Models Methods Appl. Sci., 15 (2005), 1779 - 1794.

[30] B. Hegedus, F. Marga, K. Jakab, K. L. Sharpe-Timms, G. Forgacs. *The interplay of cell-cell and cell-matrix interactions in the invasive properties of brain tumors.* Biophys. J., 91 (2006), 2708 - 2716.

[31] C. Hogea, B. Murray, J. Sethian. *Simulating complex tumor dynamics from avascular to vascular growth using a general level-set method.* J. Math. Biol., 53 (2006), 86 - 134.

[32] S. Huang, D. E. Ingber. *The structural and mechanical complexity of cell-growth control.* Nat. Cell Biol., 1 (1999), 131 - 138.

[33] E. Ising. *Beitrag zur theorie des ferromagnetismus.* Z. Physik., 31 (1925), 253.

[34] Y. Jiang, J. Pjesivac-Grbovic, C. Cantrell, J. Freyer. *A multiscale model for avascular tumor growth.* Biophys. J., 89 (2005), 3884 - 3894.

[35] H. A. Kenny, S. Kaur, L. M. Coussens, E. Lengyel. *The initial steps of ovarian cancer cell metastasis are mediated by MMP-2 cleavage of vitronectin and fibronectin.* J. Clin. Invest., 118 (2008), 1367 - 1379.

[36] G. Landini, Y. Hirayama, T. J. Li, M. Kitano. *Increased fractal complexity of the epithelial connective tissue interface in the tongue of 4NQ0-treated rats.* Pathol. Res. Pract., 196 (2000), 251 - 258.

[37] X. Li, V. Cristini, Q. Nie, J. Lowengrub. *Nonlinear three-dimensional simulation of solid tumor growth.* Discrete Dyn. Continuous Dyn. Syst. B, 7 (2007), 581 - 604.

[38] J. Lowengrub, V. Cristini, H. B. Frieboes, X. Li, P. Macklin, S. Sanga, S. M. Wise, X. Zheng. *Nonlinear modeling and simulation of tumor growth*, In N. Bellomo, M. Chaplain and E. DeAngelis Modeling and Simulation in Science, Birkaüser, in press, 2011.

[39] J. Lowengrub, V. Cristini. Multiscale modeling of cancer: an integrated experimental and mathematical modeling approach. Cambridge University Press, 2010.

[40] J. Lowengrub, H. B. Frieboes, F. Jin, Y.-L. Chuang, X. Li, P. Macklin, S. M. Wise, V. Cristini. *Nonlinear modeling of cancer: bridging the gap between cells and tumors.* Nonlinearity, 23 (2010), No. 1, R1 – R91.

[41] P. Macklin, J. Lowengrub. *An improved geometry-aware curvature discretization for level set methods: application to tumor growth.* J. Comput. Phys., 215 (2006), 392 - 401.

[42] P. Macklin, J. Lowengrub. *Nonlinear simulation of the effect of microenvironment on tumor growth.* J. Theor. Biol., 245 (2007), No. 4, 677 – 704.

[43] A. F. M. Marée, V. A. Grieneisen, P. Hogeweg, P. *The Cellular Potts Model and biophysical properties of cells, tissues and morphogenesis*. In A. R. A. Anderson, M. A. J. Chaplain, and K. A. Rejniak editors, Single-Cell-Based Models in Biology and Medicine, Mathematics and Biosciences in Interactions, Birkaüser, 107 - 136, 2007.

[44] R. M. H. Merks, P. Koolwijk. *Modeling morphogenesis in silico and in vitro: towards quantitative, predictive, cell-based modeling.* Math. Model. Nat. Phenom., 4 (2009), No. 4, 149 - 171.

[45] N. Metropolis, A. E. Rosenbluth, M. N. Rosenbluth, A. H. Teller, E. Teller. *Equation of state calculations by fast computing machines.* J. Chem. Phys., 21 (1953), 1087 - 1092.

[46] E. Montero, C. Abreu, P. Tonino. *Relationship between VEGF and p53 expression and tumor cell proliferation in human gastrointestinal carcinomas.* Journal of Cancer Research and Clinical Oncology, 134 (2007), No. 2, 193 – 201.

[47] W. Mueller-Klieser. *Tumor biology and experimental therapeutics.* Crit. Rev. Oncol. Hematol., 36 (2002), 123 - 139.

[48] G. Murphy, J. Gavrilovic. *Proteolysis and cell migration: creating a path?* Curr. Opin. Cell Biol., 11 (1999), 614 - 621.

[49] H. Osada, T. Takahashi. *Genetic alterations of multiple tumor suppressors and oncogenes in the carcinogenesis and progression of lung cancer.* Oncogene, 21 (2002), 7421 - 7434.

[50] N. B. Ouchi, J. A. Glazier, J. P. Rieu, A. Upadhyaya, J. Sawada. *Improving the realism of the cellular Potts model in simulations of biological cells.* Physica A, 329 (2003), 451 – 458.

[51] R. B. Potts. *Some generalized order-disorder transformations.* Proc. Camb. Phil. Soc., 48 (1952), 106 – 109.

[52] L. Preziosi, A. Tosin. *Multiphase modeling of tumor growth and extracellular matrix interaction: mathematical tools and applications*, J. Math. Biol., 58 (2007), No. 4-5, 625 – 656.

[53] L. Preziosi, A. Tosin. *Multiphase and multiscale trends in cancer modelling.* Math. Model. Nat. Phenom., 4 (2009), No. 3, 1 – 11.

[54] V. Quaranta, A. Weaver, P. Cummings, A. Anderson. *Mathematical modeling of cancer: The future of prognosis and treatment.* Clin. Chim. Acta, 357 (2005), 173 - 179.

[55] I. Ramis-Conde, D. Drasdo, A. R. A. Anderson, M. A. J. Chaplain. *Modeling the influence of E-cadherin-beta-catenin pathway in cancer cell invasion: a multiscale approach.* Biophys. J., 95 (2008), 155 - 165.

[56] K. A. Rejniak, R. H. Dillon. *A single cell-based model of the ductal tumor microarchitecture.* Comp. Math. Meth. Med., 8 (2007), No. 1, 51 - 69.

[57] B. Ribba, O. Sautb, T. Colinb, D. Breschc, E. Grenierd, J. P. Boissel. *A multiscale mathematical model of avascular tumor growth to investigate the therapeutic benefit of anti-invasive agents.* J. Theor. Biol., 243 (2006), 532 - 541.

[58] C. G. Rolli, T. Seufferlein, R. Kemkemer, J. P. Spatz. *Impact of Tumor Cell Cytoskeleton Organization on Invasiveness and Migration: A Microchannel-Based Approach.* PLoS ONE, 5 (2010), e8726. doi:10.1371/journal.pone.0008726.

[59] S. Sanga, J. Sinek, H. Frieboes, M. Ferrari, J. Fruehauf, V. Cristini*Mathematical modeling of cancer progression and response to chemotherapy.* Expert. Rev. Anticancer Ther., 6 (2006), 1361 - 1376.

[60] N. J. Savill, P. Hogeweg. *Modelling morphogenesis: from single cells to crawling slugs*. J. Theor. Biol., 184 (1997), 118 – 124.

[61] M. Scianna. *A multiscale hybrid model for pro-angiogenic calcium signals in a vascular endothelial cell.* Bull. Math. Biol., doi: 10.1007/s11538-011-9695-8 (2011), in press.

[62] M. Scianna, L. Preziosi. *Multiscale Developments of the Cellular Potts Model.* (2010). In revision.

[63] J. A. Smith, L. Martin. *Do cells cycle?* Proc. Natl. Acad. Sci. U.S.A., 70 (1973), 1263- 1267.

[64] J. Smolle. *Fractal tumor stromal border in a nonequilibrium growth model.* Anal. Quant. Cytol. Histol., 20 (1998), 7 - 13.

[65] I. A. Steele, R. J. Edmondson, H. Y. Leung, B. R. Davies. *Ligands to FGF receptor 2-IIIb induce proliferation, motility, protection from cell death and cytoskeletal rearrangements in epithelial ovarian cancer cell lines.* Growth Factors, 24 (2006), No. 1, 45 – 53.

[66] M. S. Steinberg. *Reconstruction of tissues by dissociated cells. Some morphogenetic tissue movements and the sorting out of embryonic cells may have a common explanation.* Science, 141 (1963), 401 – 408.

[67] M. S. Steinberg. *Does differential adhesion govern self-assembly processes in histogenesis? Equilibrium configurations and the emergence of a hierarchy among populations of embryonic cells.* J. Exp. Zool., 173 (1970), No. 4, 395 – 433.

[68] W. G. Stetler-Stevenson, S. Aznavoorian, L. A. Liotta. *Tumor cell interactions with the extracellular matrix during invasion and metastasis.* Ann. Rev. Cell Biol., 9 (1993), 541 - 573.

[69] J. L. Su, P. C. Yang, J. Y. Shih, C. Y. Yang, L. H. Wei, M. L. Kuo, et al.. *The VEGF-C/Flt-4 axis promotes invasion and metastasis of cancer cells.* Cancer Cell, 9 (2006), 209 - 223.

[70] P. Tracqui. *Biophysical models of tumour growth.* Rep. Prog. Phys., 72 (2009), No. 5, 056701.

[71] S. Turner, J. A. Sherratt. *Intercellular adhesion and cancer invasion: A discrete simulation using the extended Potts model.* J. Theor. Biol., 216 (2002), 85 – 100.

[72] P. Vaupel, M. Hockel. *Blood supply, oxygenation status and metabolic micromilieu of breast cancers: characterization and therapeutic relevance (Review).* Int. J. Oncol., 17 (2000), 869 - 879.

[73] Y. W. Zhang, G. F. Vande Woude. *HGF/SF-Met signaling in the control of branching morphogenesis and invasion.* J. Cell Biochem., 88 (2003), 408 - 417.